

Application of Tunable-slip Boundary Conditions in Particle-based Simulations

Jiajia Zhou, Jens Smiatek, Evgeny S. Asmolov, Olga I. Vinogradova, and Friederike Schmid

Abstract Compared to macroscopic systems, fluids on the micro- and nanoscales have a larger surface-to-volume ratio, thus the boundary condition becomes crucial in determining the fluid properties. No-slip boundary condition has been applied successfully to wide ranges of macroscopic phenomena, but its validity in microscopic scale is questionable. A more realistic description is that the flow exhibits slippage at the surface, which can be characterized by a Navier slip length. We present a tunable-slip method by implementing Navier boundary condition in particle-based computer simulations (Dissipative Particle Dynamics as an example). To demonstrate the validity and versatility of our method, we have investigated two model systems: (i) the flow past a patterned surface with alternating no-slip/partial-slip stripes and (ii) the diffusion of a spherical colloidal particle.

Jiajia Zhou

Institut für Physik, Johannes Gutenberg-Universität Mainz, Staudingerweg 7, D-55099 Mainz, Germany, e-mail: zhou@uni-mainz.de

Jens Smiatek

Institut für Computerphysik, Universität Stuttgart, Allmandring 3, 70569 Stuttgart, Germany

Evgeny S. Asmolov

A.N. Frumkin Institute of Physical Chemistry and Electrochemistry, Russian Academy of Science, 31 Leninsky Prospect, 119071 Moscow, Russia

Central Aero-Hydrodynamic Institute, 140180 Zhukovsky, Moscow region, Russia

Institute of Mechanics, M.V. Lomonosov Moscow State University, 119991 Moscow, Russia

Olga I. Vinogradova

A.N. Frumkin Institute of Physical Chemistry and Electrochemistry, Russian Academy of Science, 31 Leninsky Prospect, 119071 Moscow, Russia

Department of Physics, M.V. Lomonosov Moscow State University, 119991 Moscow, Russia

DWI - Leibniz Institute for Interactive Materials, RWTH Aachen, Forckenbeckstraße 50, 52056 Aachen, Germany

Friederike Schmid

Institut für Physik, Johannes Gutenberg-Universität Mainz, Staudingerweg 7, D-55099 Mainz, Germany, e-mail: friederike.schmid@uni-mainz.de

1 Introduction

Modeling fluids in small length scales from micrometer to nanometer not only is a fundamental problem in fluid mechanics, but also plays a paramount role in modern fluidic devices [1]. These micro- or nanofluidic devices can be found in wide range of applications and in many different fields. Examples include the development of inkjet printheads for xerography, lab-on-a-chip technology, and manipulation and separation of bio-molecules. Compared to macroscopic systems, microscopic fluids have a larger surface-to-volume ratio, therefore boundary conditions become crucial in determining the hydrodynamic properties. The most well-known boundary condition is the no-slip boundary condition, i.e., the fluid velocity vanishes at a fluid/solid interface. No-slip boundary condition has been successfully applied to wide ranges of macroscopic phenomena, but it has no microscopic justification and its validity in small length scales is questionable. A more general boundary condition is the Navier boundary condition, which is described in the following.

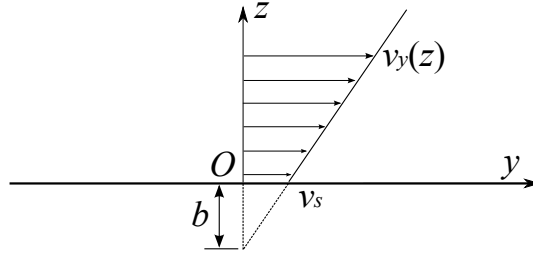


Fig. 1 Schematic representation of Navier boundary condition on a flat surface and the slip length.

Assume that a fluid/solid interface lies in the xOy plane and the fluid occupies $z > 0$ half-space (Fig. 1). Let us consider the case of a laminar Couette flow in the y -direction, with a slip velocity v_s at $z = 0$. The tangential force per unit area (component of the shear stress σ_{yz}), to the first-order approximation, is proportional to the slip velocity v_s ,

$$\sigma_{yz} = \zeta_s v_s, \quad (1)$$

where ζ_s is the surface friction coefficient. For Newtonian fluids, the shear stress can also be written as

$$\sigma_{yz} = \eta \frac{\partial v_y}{\partial z}, \quad (2)$$

where η is the shear viscosity of the fluid. Combining Eq. (1) and (2), one arrives the Navier boundary condition [2]

$$v_s = \frac{\eta}{\zeta_s} \frac{\partial v_y}{\partial z} = b \frac{\partial v_y}{\partial z}. \quad (3)$$

The degree of slippage at the surface is quantified in terms of the Navier slip length $b = \eta/\zeta_s$. No-slip boundary condition is recovered for $b = 0$, while for ideal frictionless surface we have $b \rightarrow \infty$. The physical meaning of the slip length is the distance within the solid at which the flow velocity extrapolates to zero.

2 Implementation

The main question we try to address in this contribution is the implementation of Navier boundary condition with tunable slip length in particle-based computer simulations. Any models of a solid surface require at least two components: (a) an excluded interaction to prevent fluid particles penetrating the hard surface; and (b) an effective interaction due to the surface friction. In the following, we shall use Dissipative Particle Dynamics (DPD) [3, 4, 5] to demonstrate the tunable-slip method, although the basic idea is quite general and can be applied to other simulation techniques. In the following we only give a brief description and introduce parameters for later discussions. For a more detailed description, please consult the origin reference [6].

We model the impermeable surface using a pure repulsive interaction of the Weeks-Chandler-Andersen form [7],

$$V(z) = \begin{cases} 4\epsilon[(\frac{\sigma}{z})^{12} - (\frac{\sigma}{z})^6 + \frac{1}{4}], & z < \sqrt[6]{2}\sigma \\ 0, & z \geq \sqrt[6]{2}\sigma \end{cases} \quad (4)$$

where z is the distance between the fluid particle and the wall. The WCA parameters also set the unit system (ϵ for the energy, σ for the length, and m for the particle mass).

The interactions between the surface and fluid can be very complicated and depend on the chemical details. But in the mesoscale, the main effect of the surface is to provide friction. Inspired by the form of Eq. (1), we model the fluid/surface friction by a dissipative force to the fluid, which depends on the relative velocity between the fluid particle and the wall,

$$\mathbf{F}_i^D = -\gamma_L \omega_L(z)(\mathbf{v}_i - \mathbf{v}_{\text{wall}}). \quad (5)$$

The friction constant γ_L is an adjustable parameter that characterizes the strength of the wall friction, and it can be used to vary the slip length. The position-dependent function $\omega_L(z)$ is a monotonically decreasing function of the wall-particle separation, and vanishes at certain cutoff z_c to mimic the finite range of the wall interaction. Additionally, a random force obeying the fluctuation-dissipation theorem is required to ensure the correct equilibrium statistics,

$$\mathbf{F}_i^R = \sqrt{2k_B T \gamma_L \omega_L(z)} \xi_i, \quad (6)$$

where k_B is the Boltzmann constant, T the temperature, and ξ_i a vector whose component is a Gaussian distributed random variable with zero mean and unit variance.

The slip length b can be computed analytically as a function of a dimensionless parameter $\alpha = z_c^2 \gamma_L \rho / \eta$, where ρ is the fluid number density [6]. For a linear function $\omega_L(z) = 1 - z/z_c$, the relation is

$$\frac{b}{z_c} = \frac{2}{\alpha} - \frac{7}{15} - \frac{19}{1800} \alpha + \dots \quad (7)$$

This formula works quite well for large values of b , but shows deviation near the no-slip region ($b/\sigma \sim 1$). The slip length can also be measured by short simulations of Poiseuille and Couette flow in a thin channel geometry. Fig. 2 shows the relation between the slip length b and the wall friction parameter γ_L . One can then choose a suitable value of γ_L based on the requirement of the slip length.

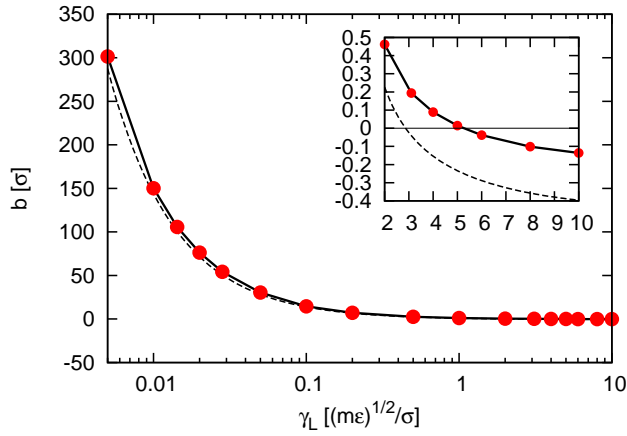


Fig. 2 Relation between the slip length b and the wall friction parameter γ_L . The inset shows an enlarged portion of the region where the slip length is zero. No-slip boundary condition can be implemented by using $\gamma_L = 5.26\sqrt{m\varepsilon}/\sigma$. Dashed curves show analytical prediction Eq. (7).

To demonstrate the validity and versatility of our method, we investigate two model systems: the flow past a patterned surface with alternating no-slip/partial-slip stripes (Section 3) and free diffusion of a slipping colloidal particle (Section 4).

3 Striped Surfaces

Patterned surfaces play a major role in micro- and nanofluidics. One important example is the superhydrophobic Cassie surfaces, where no-slip and partial-slip area arrange in a striped pattern [see Fig. 3(a)]. The no-slip region consists of fluid/solid

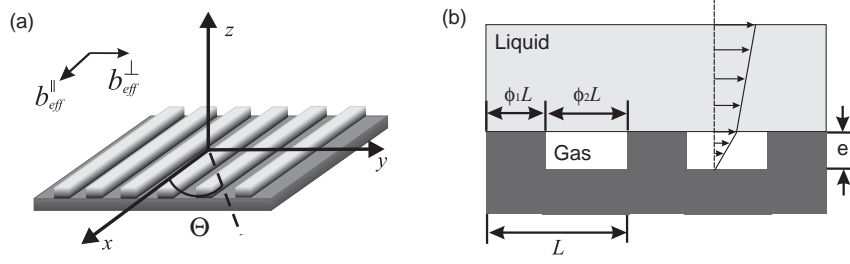


Fig. 3 Sketch of the striped surface: $\Theta = 0$ to longitudinal stripes, $\Theta = \pi/2$ corresponds to transverse stripes (a), and of the liquid interface in the Cassie state (b).

interface, while the partial-slip region consists of trapped gas which is stabilized by a rough wall texture. These superhydrophobic surfaces exhibit very low friction, and the drag reduction is associated with the large slip length over the fluid/gas interfaces.

We simulate the superhydrophobic Cassie surface using the “gas-cushion model” [8]. Instead of modeling the physically corrugated surface, we use a *flat* surface with alternating no-slip and partial-slip boundary conditions. The value of the slip length b over the gas sector is related to the thickness of the gas region e by

$$b \simeq \frac{\eta}{\eta_g} e, \quad (8)$$

where η and η_g are shear viscosities of a gas and a liquid [see Fig. 3(b)]. We consider a striped pattern with a periodicity L . The area fractions of the solid and gas sectors are ϕ_1 and ϕ_2 , respectively. For inhomogeneous surfaces, the effective slip length depends on the flow direction Θ and is in general a tensorial quantity \mathbf{b}_{eff} . For the special case of striped surfaces, the eigenvalues of the slip length tensor correspond to the flow direction parallel to the stripes (maximum slip $b_{\text{eff}}^{\parallel}$) and perpendicular to the stripes (minimum slip b_{eff}^{\perp}).

We compare our simulation results with the numerical solution to the Stokes equations and some analytical formulas. The results for the perfect-slip gas sector ($b \gg L$) are well-known [9, 10]

$$\frac{b_{\text{eff}}^{\parallel}}{L} = \frac{2b_{\text{eff}}^{\perp}}{L} \simeq \frac{1}{\pi} \ln \left[\sec \left(\frac{\pi\phi_2}{2} \right) \right]. \quad (9)$$

For arbitrary value of b , Belyaev and Vinogradova suggested approximate expressions [11],

$$\frac{b_{\text{eff}}^{\parallel}}{L} \simeq \frac{1}{\pi} \frac{\ln \left[\sec \left(\frac{\pi \phi_2}{2} \right) \right]}{1 + \frac{L}{\pi b} \ln \left[\sec \left(\frac{\pi \phi_2}{2} \right) + \tan \left(\frac{\pi \phi_2}{2} \right) \right]}, \quad (10)$$

$$\frac{b_{\text{eff}}^{\perp}}{L} \simeq \frac{1}{2\pi} \frac{\ln \left[\sec \left(\frac{\pi \phi_2}{2} \right) \right]}{1 + \frac{L}{2\pi b} \ln \left[\sec \left(\frac{\pi \phi_2}{2} \right) + \tan \left(\frac{\pi \phi_2}{2} \right) \right]}. \quad (11)$$

These formulas are accurate over wide range of the parameters and recover to Eq. (9) at large b value.

We start with varying Θ for patterns that has equal areas of no-slip and partial-slip regions ($\phi_2 = 0.5$) and the slip length is in the intermediate region $b/L = 1.0$. Figure 4 shows the results for the effective downstream slip lengths, $b_{\text{eff}}(\Theta)$, and the theoretical curve

$$b_{\text{eff}}(\Theta) = b_{\text{eff}}^{\parallel} \cos^2 \Theta + b_{\text{eff}}^{\perp} \sin^2 \Theta. \quad (12)$$

The simulation data are in good agreement with theoretical predictions, confirming the anisotropy of the flow and the validity of the concept of a tensorial slip for striped surfaces.

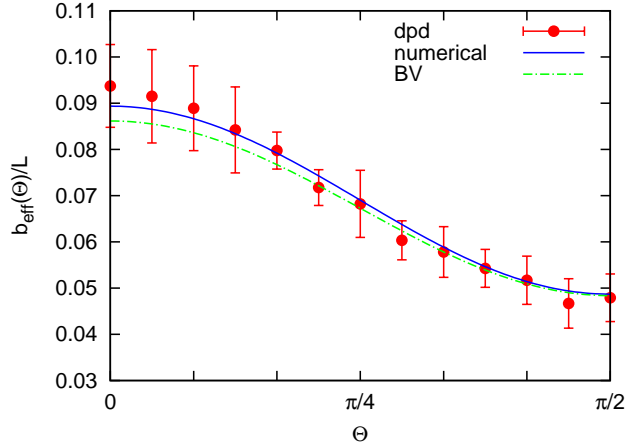


Fig. 4 Effective downstream slip length, $b_{\text{eff}}(\Theta)$ as a function of tilt angle Θ for a pattern with $b/L = 1.0$ and $\phi_2 = 0.5$. Symbols with error bars are simulation data. Curves are theoretical values calculated using Eq. (12) with eigenvalues obtained by a numerical method (solid) and by Eqs. (10,11) (dot-dashed).

Next we examine the effect of varying the fraction of gas/liquid interface, ϕ_2 . Figure 5(a) shows the effective slip lengths $b_{\text{eff}}^{\parallel}$ and b_{eff}^{\perp} as a function of ϕ_2 . The

striped pattern again has $b/L = 1.0$. The results clearly demonstrate that the gas fraction ϕ_2 is the main factor in determining the value of effective slip; the slip length increases significantly when the gas fraction increases to unity.

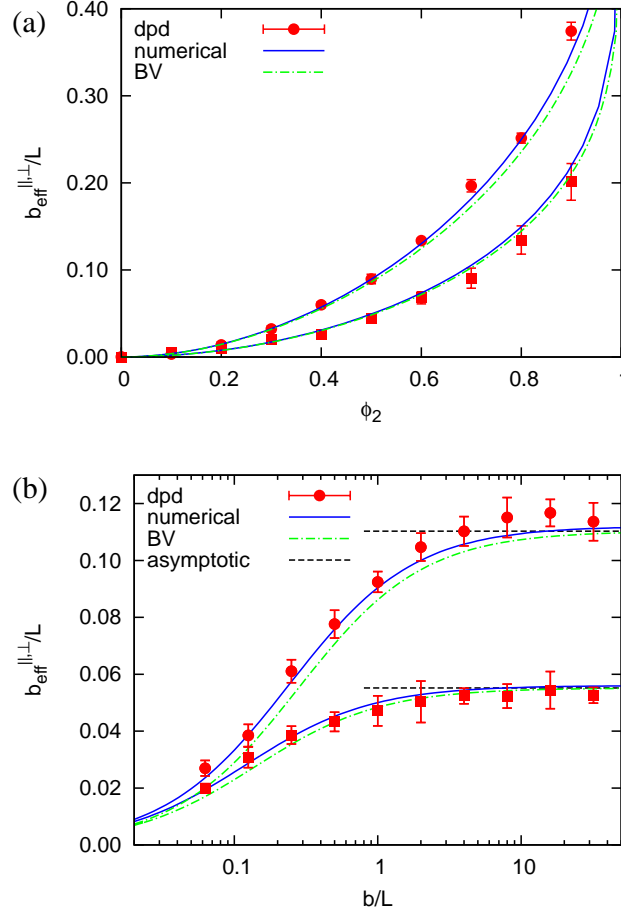


Fig. 5 (a) Effective slip lengths (symbols) as a function of gas-sector fraction ϕ_2 for $b/L = 1.0$. (b) Effective slip lengths as a function of local slip length b for $\phi_2 = 0.5$. The numerical results are shown as solid curves. Also shown are analytic expressions Eqs. (10,11) (dot-dashed), and asymptotic formulas Eq. (9) (dashed lines, for (b) only).

Finally, we present the effective slip lengths as a function of the local slip length b at gas/liquid interface in Fig. 5(b). The pattern has equal fractions of solid and gas, $\phi_1 = \phi_2 = 0.5$. The analytic formulas Eqs. (10,11) are shown in dot-dashed lines, which are accurate over wide range of b value. The effective slip lengths reach the asymptotic values predicted by Eq. (9) at large values of b/L . The excellent agreement between the simulation data and theoretic predictions promotes studies

of more complex systems and applications, such as thin channels with symmetric stripes [12], anisotropic flow over weakly slipping stripes [13], trapezoidal grooves [14], electroosmotic flows [15], polyelectrolyte electrophoresis [16, 17], and separation of chiral particles [18].

4 Colloidal Particle

Colloidal dispersions have numerous applications in different fields such as chemistry, biology, medicine, and engineering [19, 20]. Better understanding of the dynamics of colloidal particles can provide insights to improve the material properties. Molecular simulations can shed light on the dynamic phenomena of colloidal particles in a well-defined model system. Due to the size difference between the colloids and solvent molecules, it is difficult to simulate the system on the smaller length scale (the solvent), and one has to rely on coarse-graining technique to reach meaningful time scales. The general idea is to couple the solute with a mesoscopic model for Navier-Stokes fluids. One of the examples is the coupling scheme developed by Ahlrichs and Dünweg [21], which combines a Lattice-Boltzmann approach for the fluid and a continuum Molecular Dynamics model for the polymer chains. The method has been extended to colloidal particles [22, 23]. We shall discuss a similar colloid model based on DPD.

The interactions between the colloid and fluid can be separated into two components, similar to the case of flat surface presented in Section 2. One component is the hard-core interaction to prevent the fluid entering the colloid. We use a pure repulsive potential of WCA form [Eq. (4)]. The other one is the friction between the colloid surface and the fluid, which can be modeled by a pair of dissipative and random forces [cf. Eqs. (5, 6)]. The complication arises for colloidal particles which have a curved surface. There are two possible solutions. The first is to treat the surface as a continuous two-dimensional object and replace z in the friction force pair by the shortest distance between the fluid particle and the curved surface. This can be easily implemented for simple geometry such as spheres, but becomes complicated for colloids with irregular shape. The second solution is to discretize the surface by many interaction sites, whose positions are fixed in the local frame of the colloid. These sites interact with the solvent through the DPD dissipative and stochastic interactions, with a friction coefficient γ_L [Eqs. (5, 6) but with z replaced by bead separation r]. Boundary conditions on the colloid surface can be tuned by vary the value of γ_L . In this work, we opt to the second option for better extensibility. Fig. 6 shows a representative snapshot of a colloidal particle decorated by many surface sites.

The total force exerted on the colloid is given by the sum over all forces on the surface sites, plus the conservative excluded volume interaction,

$$\mathbf{F}_C = \sum_{i=1}^N [\mathbf{F}_i^D(\mathbf{r}_i) + \mathbf{F}_i^R(\mathbf{r}_i)] + \mathbf{F}^{\text{WCA}}. \quad (13)$$

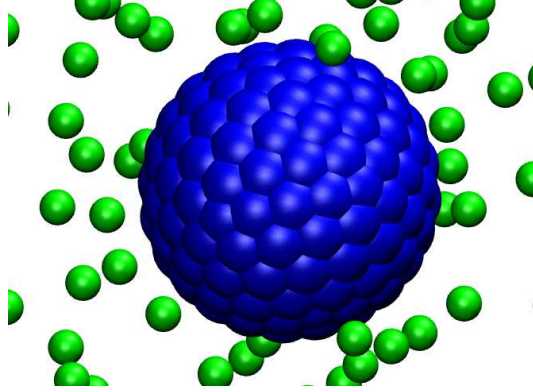


Fig. 6 Snapshot of a colloidal particle in solution. The surface sites are represented by the dark beads, and the light beads are fluid particles. Only selective solvent beads are shown here for clarity.

Here \mathbf{r}_i denotes the position of i -th surface sites and there are N of them. Similarly, the torque exerted on the colloid can be written as

$$\mathbf{T}_C = \sum_{i=1}^N [\mathbf{F}_i^D(\mathbf{r}_i) + \mathbf{F}_i^R(\mathbf{r}_i)] \times (\mathbf{r}_i - \mathbf{r}_{cm}), \quad (14)$$

where \mathbf{r}_{cm} is the position of the colloid's center-of-mass. Note that the excluded volume interaction does not contribute to the torque because the associated force points towards the center for spherical colloids, but this is in general not true for irregular shape. The total force and torque are then used to update the position and velocity (both translational and rotational) of the colloid at the next time step.

The diffusion constant of the colloid can be calculated from the velocity autocorrelation function using the Green-Kubo relation or by a linear fit to the mean-square displacement. Due to the periodic boundary condition implemented in simulations, the diffusion constant for a single colloid in a finite simulation box depends on the box size. Fig. 7(a) demonstrates the finite-size effect by plotting the mean-square displacement as a function of time for two different simulation boxes $L = 10\sigma$ and $L = 30\sigma$.

The diffusion constant increases with increasing box size. For small simulation box, the long-wavelength hydrodynamic modes are suppressed due to the coupling between the colloid and its periodic images. The diffusion constant can be written in terms of an expansion of $1/L$, the reciprocal of the box size [24]

$$D = \frac{k_B T}{6\pi\eta} \left(\frac{1}{R} - \frac{2.837}{L} + \frac{4.19R^2}{L^3} + \dots \right). \quad (15)$$

In Fig. 7(b), simulation results of the diffusion constant are plotted in terms of $1/L$. The simulation results and the hydrodynamic theory show reasonable agreement.

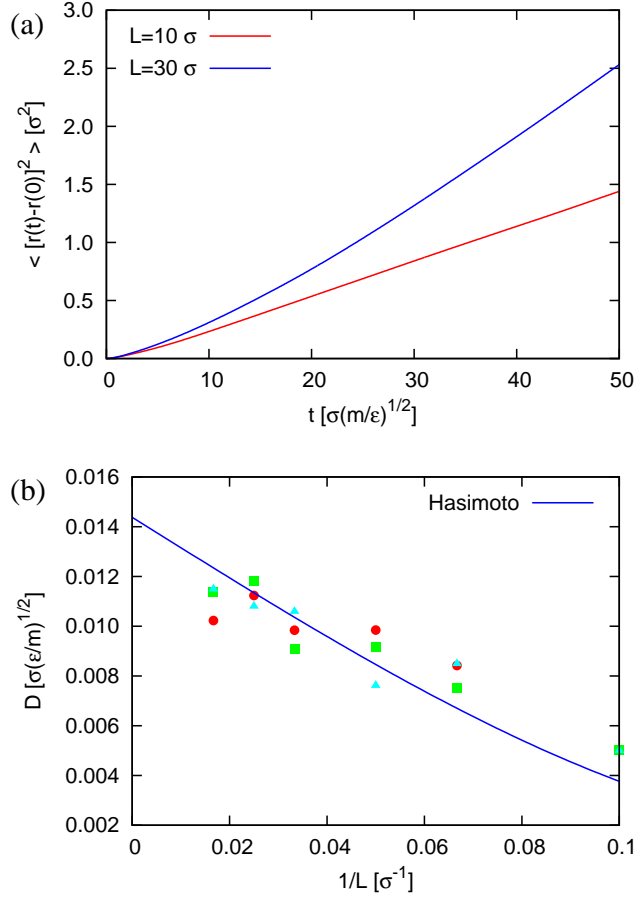


Fig. 7 (a) Mean-square displacement of a spherical colloid with radius $R = 3.0\sigma$ for two different sizes of simulation box, $L = 10\sigma$ and $L = 30\sigma$. (b) Diffusion constant D for a spherical colloid of radius $R = 3.0\sigma$ as a function of the reciprocal of the box size $1/L$. The curve is the prediction from Eq. (15). Different symbols correspond to simulation runs with different initialization.

Most of the studies on colloid dynamics have been focus on the no-slip boundary condition. We have investigated the response of charged colloids under alternating electric fields [25, 26, 27, 28]. No-slip is valid for large colloids, but may be questionable for nanometer-sized or hydrophobic particles. Furthermore, one can adjust the boundary condition by modifying the surface properties. One advantage of our colloid model is the ability to adjust the boundary condition from no-slip to full-slip by changing the friction coefficient γ_L . Fig. 8 illustrates the change of the diffusion constant by varying γ_L in a simulation box $L = 30\sigma$. This freedom provides opportunities to study the effect of hydrodynamic slip on the colloid dynamics [29, 30].

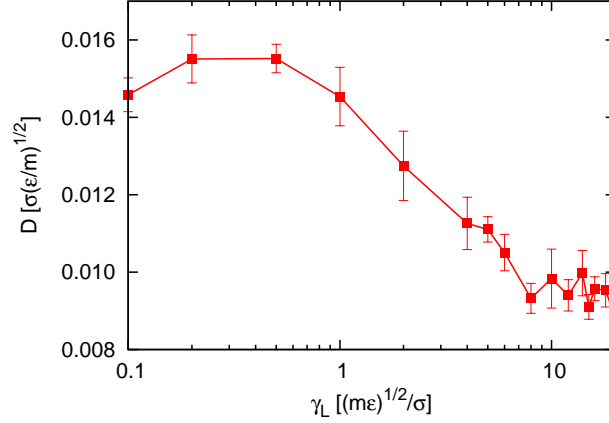


Fig. 8 Diffusion constant D for a spherical colloid of radius $R = 3.0\sigma$ as a function of the surface-fluid DPD friction coefficient γ_L . The simulation box has a size of $L = 30\sigma$. No-slip is realized for $\gamma_L > 10\sqrt{m\varepsilon}/\sigma$.

5 Summary

We have presented a coarse-grained method to implement Navier boundary condition with arbitrary slip length in particle-based simulations. We have validated our method by simulating a flat homogeneous surface and proposed an analytical relation between the slip length and simulation parameters. To illustrate the versatility of the method, we extend the method to inhomogeneous surfaces by investigating Newtonian flow over superhydrophobic striped surface, and to curved surfaces by studying the dynamics of single spherical colloid. Our method provides a general tool to exam the slip-dependent phenomena in particle-based simulations and should be suitable to study more complex system, for example, flow over structured surface or channel and dynamics of aspherical colloids.

Acknowledgements

We thank the HLRS Stuttgart for a generous grant of computer time on HERMIT. This research was supported by the DFG through the SFB TR6, SFB 985, SFB 1066, and by RAS through its priority program ‘‘Assembly and Investigation of Macromolecular Structures of New Generations’’.

References

1. T.M. Squires, S.R. Quake, *Rev. Mod. Phys.* **77**, 977 (2005)
2. L. Bocquet, J.L. Barrat, *Soft Matter* **3**, 685 (2007)
3. P.J. Hoogerbrugge, J.M.V.A. Koelman, *Europhys. Lett.* **19**, 155 (1992)
4. P. Español, P.B. Warren, *Europhys. Lett.* **30**, 191 (1995)
5. R.D. Groot, P.B. Warren, *J. Chem. Phys.* **107**, 4423 (1997)
6. J. Smiatek, M. Allen, F. Schmid, *Eur. Phys. J. E* **26**, 115 (2008)
7. J.D. Weeks, D. Chandler, H.C. Andersen, *J. Chem. Phys.* **54**, 5237 (1971)
8. O.I. Vinogradova, *Langmuir* **11**, 2213 (1995)
9. J.R. Philip, *J. Appl. Math. Phys.* **23**, 353 (1972)
10. E. Lauga, H.A. Stone, *J. Fluid Mech.* **489**, 55 (2003)
11. A.V. Belyaev, O.I. Vinogradova, *J. Fluid Mech.* **652**, 489 (2010)
12. J. Zhou, A.V. Belyaev, F. Schmid, O.I. Vinogradova, *J. Chem. Phys.* **136**, 194706 (2012)
13. E.S. Asmolov, J. Zhou, F. Schmid, O.I. Vinogradova, *Phys. Rev. E* **88**, 023004 (2013)
14. J. Zhou, E.S. Asmolov, F. Schmid, O.I. Vinogradova, *J. Chem. Phys.* **139**, 174708 (2013)
15. J. Smiatek, M. Sega, C. Holm, U.D. Schiller, F. Schmid, *J. Chem. Phys.* **130**, 244702 (2009)
16. J. Smiatek, F. Schmid, *J. Phys. Chem. B* **114**, 6266 (2010)
17. J. Smiatek, F. Schmid, *Comput. Phys. Commun.* **182**, 1941 (2011)
18. S. Meinhardt, J. Smiatek, R. Eichhorn, F. Schmid, *Phys. Rev. Lett.* **108**, 214504 (2012)
19. W.B. Russel, D.A. Saville, W. Schowalter, *Colloidal Dispersions* (Cambridge University Press, Cambridge, 1989)
20. J. Dhont, *An Introduction to Dynamics of Colloids* (Elsevier, Amsterdam, 1996)
21. P. Ahlrichs, B. Dünweg, *J. Chem. Phys.* **111**, 8225 (1999)
22. V. Lobaskin, B. Dünweg, *New Journal of Physics* **6**, 54 (2004)
23. A. Chatterji, J. Horbach, *J. Chem. Phys.* **122**, 184903 (2005)
24. H. Hasimoto, *J. Fluid Mech.* **5**, 317 (1959)
25. J. Zhou, F. Schmid, *J. Phys.: Condens. Matter* **24**, 464112 (2012)
26. J. Zhou, F. Schmid, *Eur. Phys. J. E* **36**, 33 (2013)
27. J. Zhou, R. Schmitz, B. Dünweg, F. Schmid, *J. Chem. Phys.* **139**, 024901 (2013)
28. J. Zhou, F. Schmid, *Eur. Phys. J. Special Topics* **222**, 2911 (2013)
29. J.W. Swan, A.S. Khair, *J. Fluid Mech.* **606**, 115 (2008)
30. A.S. Khair, T.M. Squires, *Phys. Fluids* **21**, 042001 (2009)